
Interactive comment on “Observations and explicit modeling of isoprene chemical processing in polluted air masses in rural areas of the Yangtze River Delta region: radical cycling and formation of ozone and formaldehyde” by Kun Zhang et al.

Response to Referee #1

Received and published: 29 September 2020

Major comments

I find two main issues with the analysis presented in sections 3.2 and 3.3. One is the lack of heterogeneous chemistry in the model. This is likely to impact both the levels and the budget of OH (because of the heterogeneous sources of HONO), of HO₂ (because of HO₂ uptake on aerosol), and of NO₃ (because of the equilibrium with N₂O₅). I don't think that a complete analysis of radical chemistry can just ignore these processes. If the authors think that heterogeneous chemistry is negligible under the conditions of this study (and it may well be so), they should provide some evidence or reason why that is the case.

Response: We really appreciate the reviewers careful and valuable comments. We agree that the heterogeneous processes associated with HONO source, uptake of HO₂ and N₂O₅ could be important for the budget of OH, HO₂ and NO₃ under certain conditions. Therefore, we tested the heterogeneous processes including uptake of N₂O₅, HCHO, and HO₂ on aerosols surface, and heterogenous sources of HONO in our simulation, as summarized in Table 1. Rate constants and uptake coefficients for these reactions were obtained from previous studies (Riedel et al. (2014); Xue et al. (2014); Li et al. (2014)). Since key parameters such as aerosol surface areas (S_A) were not directly measured during our observation period, an average value of S_A (640 nm²/cm³ from the study of Wang et al. (2014)) was adopted in this study. Our results suggest that adding heterogenous processes in our simulation could lead to decrease of OH, HO₂, RO₂ and NO₃ by 1.53%, 4.54%, 2.73%

and 6.53%, respectively. These processes have been included in our base simulation and results are updated accordingly.

Table 1. Additional heterogenous reactions and associated rate constants used by the model

Reactions	Rate constants	No.
$N_2O_5 \rightarrow CLNO_2 + HNO_3$	$\gamma\omega S_A/4$ (for $CLNO_2$ formation) $(2 - \phi)\gamma\omega S_A/4$ (for HNO_3 formation)	Riedel et al. (2014)
$NO_2 \rightarrow HONO$	$k_g = \frac{1}{8} \times \omega\gamma\left(\frac{S}{V}\right)$ $k_a = \frac{1}{4} \omega\gamma S_A$	Xue et al. (2014)
$HO_2 \rightarrow products$	$k = \left(\frac{r}{D_g} - \frac{4}{\gamma}\omega\right)^{-1} S_A$	Xue et al. (2014)
$HCHO \rightarrow products_1$	$k = \frac{1}{4} \omega\gamma S_A$	Li et al. (2014)

γ = uptake coefficient for the given reactant with aerosol surface area; ϕ = product yield; ω =mean molecular speed of the given reactant (m/s); S_A =RH corrected aerosol surface area concentration (nm^2/cm^3); r =surface-weighted particle radius.

References:

- Li, X., Rohrer, F., Brauers, T., Hofzumahaus, A., Lu, K., Shao, M., Zhang, Y. H., and Wahner, A. (2014). Modeling of HCHO and CHOCHO at a semi-rural site in southern China during the PRIDE-PRD2006 campaign, *Atmospheric Chemistry and Physics*, 14, 12291-12305, 10.5194/acp-14-12291-2014.
- Riedel, T. P., Wolfe, G. M., Danas, K. T., Gilman, J. B., Kuster, W. C., Bon, D. M., Vlasenko, A., Li, S.-M., Williams, E. J., Lerner, B. M., Veres, P. R., Roberts, J. M., Holloway, J. S., Lefer, B., Brown, S. S., and Thornton, J. A. (2014). An MCM modeling study of nitryl chloride ($ClNO_2$) impacts on oxidation, ozone production and nitrogen oxide partitioning in polluted continental outflow, *Atmos. Chem. Phys.*, 14, 3789–3800, <https://doi.org/10.5194/acp-14-3789-2014>.

Xue, L., Wang, T., Gao, J., Ding, A., Zhou, X., Blake, D. R., Fang, X., Saunders, S. M., Fan, S., Zuo, H., Zhang, Q., Wang, W. (2014). Ground-level ozone in four Chinese cities: precursors, regional transport and heterogeneous processes. *Atmospheric chemistry and physics*, 14(23), 13175-13188.

Wang, X., Chen, J., Cheng, T., Zhang, R., Wang, X. (2014) Particle number concentration, size distribution and chemical composition during haze and photochemical smog episodes in Shanghai[J]. *Journal of Environmental Sciences*, 26(009):1894-1902.

The other important issue is the HONO/NO₂ ratio which is set here to 2%, based on the Tan et al., 2019 paper. However that study examined Chinese megacities and I would expect HONO and NO₂ levels to be different in rural areas. I appreciate that without HONO measurements it is not possible to be very accurate on this point, but since the paper shows that HONO is a major source of OH, this issue should be discussed somewhere in the manuscript. I suggest at least a sensitivity study to assess how the estimate of HONO impacts the model results and hence the conclusions of the paper. If, on the other hand, the conditions in this study and in the Tan et al., 2019, paper are similar, that would bring into question the classification of the measurement site as "rural", which would necessarily reframe the subject and the conclusions of the paper.

Response: We agree that the HONO/NO₂ ratio in this study is different from that in Tan et al. (2019). To investigate the sensitivity of our results to the HONO/NO₂ ratio, a series of simulations with different HONO/NO₂ ratios were conducted and the results were summarized in Table 2. A lower HONO/NO₂ ratio (e.g. 0.005) could lead to decrease of OH radical by 15.3% and a higher ratio (e.g. 0.04) could increase OH concentration by

14.1%. This could be explained by the important role of HONO photolysis as one of the OH sources. Discussions on the sensitivity results have been added to the revised manuscript (Page 13, Line 258-266):

“Sensitive studies were conducted to quantify the influences of different HONO/NO₂ ratios on radical recycling (Text S3, Figure. S1 and Table S1). As expected, lower HONO/NO₂ ratio leads to lower HONO concentrations, and subsequent less OH generated from the photolysis of HONO. The sensitive study shows that when HONO/NO₂ ratio is 0.005, the daytime OH level could decrease by 15.3%. Vice versa, a higher HONO/NO₂ ratio (e.g., 0.04) can promote OH concentration by 14.08%. This result indicates that the photolysis of HONO is essential to the generation of OH, and therefore a simultaneous measurement of HONO is highly recommended for analyzing local radical recycling.”

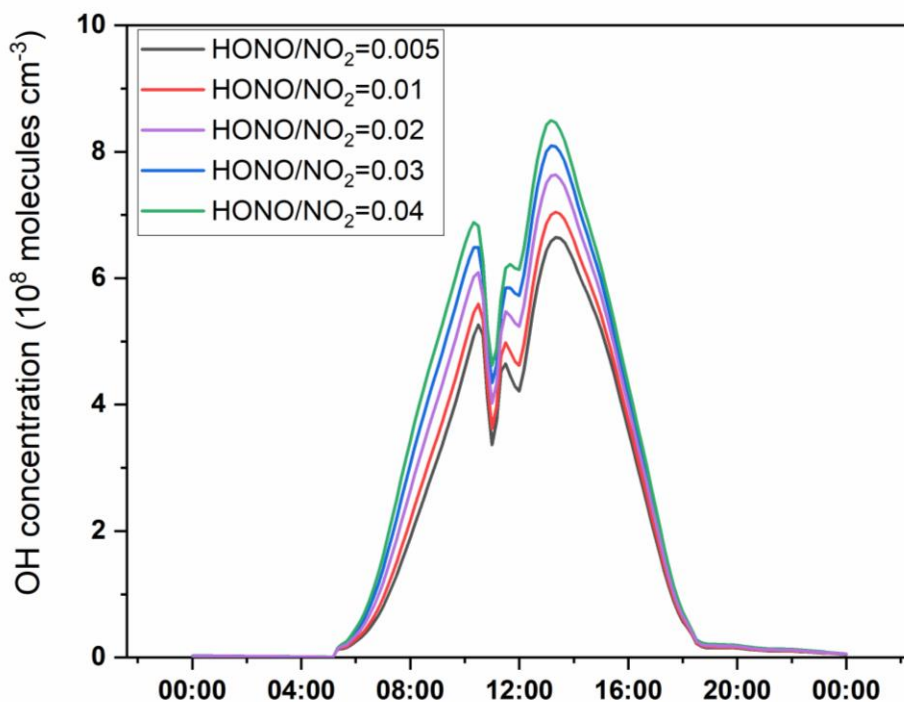


Fig. 1 Comparison of OH concentration under different HONO/NO₂ ratios.

Table 2 Model sensitivity test result.

HONO/NO ₂ ratio	Change in OH (%)
0.005	-15.3%
0.01	-9.3%
0.03	7.5%
0.04	14.1%

With regards to the analysis of ozone and formaldehyde I am confused about the model setup. On line 141 it is said that O₃, NO_x and VOCs (does it include HCHO?) are constrained in the model. However, on lines 147-151 and in Figure S1, "simulated ozone" is discussed. It is also not clear if HCHO is constrained or not. A species can be either constrained or calculated (simulated) in a model, but not both. The larger point, however, is that if O₃ and/or HCHO are constrained, then the results in sections 3.4, 3.5, 3.6.2 and 3.6.3 need to be revised. It does not make much sense to look at the rate of production of a constrained variable because its value is set by the model and not calculated based on the values of the other variables. So the authors should first clarify whether O₃ and HCHO are constrained or calculated in the model and then amend the discussion in sections 3.4, 3.5, 3.6.2 and 3.6.3 accordingly.

Response: O₃ and HCHO were not constrained in our simulation, because we want to analyze the secondary formation of these compounds. To avoid misunderstanding, we have revised related descriptions in the revised manuscript (Line 146-147): " Hourly averaged concentrations of speciated VOCs (except HCHO), NO, NO₂ and meteorological parameters (such as T, RTH, P) were used to constrain the F0AM model."

Minor comments

In Table 1, and in the related text, I believe "42i" and "43i" need to be exchanged. Also, I suggest the detection limits and/or uncertainties are added to the Table 1.

Response: Thanks for the helpful advice. We have exchanged "42i" and "43i" in Table 1 and in the related text and add detection limits in Table 1.

line 103: correct to "Vaisala"

Response: We have corrected "Visala" into "Vaisala"

line 115: I imagine you mean 15m above the 5th floor?

Response: We are sorry for the unclear expression, and we mean the top of the 5-floor-high building is 15 m above the ground level. Therefore, we have revised this sentence into "The instruments were housed on the top of a 5-floor-high building, which was about 15 m above the ground level."

line 142: correct to "RH".

Response: We have revised this word as suggested.

lines 143: correct to "nitrous acid".

Response: We have revised this word as suggested.

line 149: please define these indices (IOA, MB, NMB).

Response: The definition of IOA, MB and NMB are given in Line 153-157: “The index of agreement (IOA) , mean bias (MB) and normalized mean bias (NMB) are frequently used to estimate the model performance. These three parameters can be calculated by Equation (2) to (4), where S_i , O_i , and \bar{O} are the simulated, observed, and average value of the target compound. “

$$IOA = 1 - \frac{\sum(S_i - O_i)^2}{\sum(|S_i - \bar{O}| + |O_i - \bar{O}|)^2} \quad (2)$$

$$MB = \frac{\sum(S_i - O_i)}{N} \quad (3)$$

$$NMB = \frac{\sum(S_i - O_i)}{\sum O_i} \times 100 \quad (4)$$

lines 199-201: I assume you are talking about simulated NO₃ here. Please always make clear in the text, figures and captions, when you are talking about measurements and when about model results.

Response: Thanks for the reviewer’s valuable suggestion. We have specified the “simulated NO₃” in Line 236-237. In addition, we have checked the similar unclear expression throughout the paper.

lines 205-207: I am not aware of RO+NO₃ reactions forming RO₂. Can you please clarify and/or correct?

Response: We are sorry for this mistake. It should be the reaction of VOCs+NO₃ that account for over 70% RO₂ production during nighttime, and relevant description has been revised.

line 212: correct to "ozonolysis".

Response: We have corrected this error as suggested.

1 **Response to Referee #2**

2 Received and published: 23 October 2020

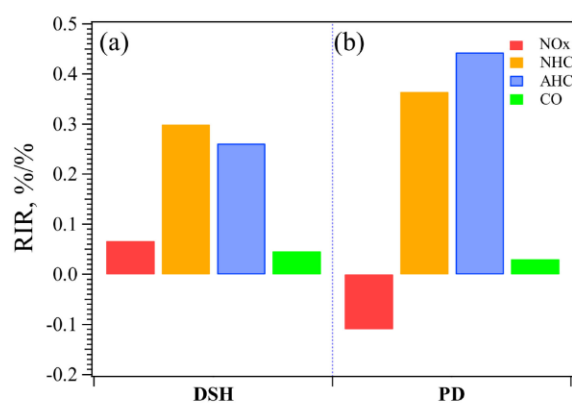
3 1) The title of manuscript “Observations and explicit modeling of isoprene chemical processing
4 in polluted air masses in rural areas of the Yangtze River Delta region: radical cycling and
5 formation of ozone and formaldehyde” is not well supported by the work presented. The
6 observations are limited since key product species (i.e., MACR and MVK) and RO_x radicals
7 of isoprene were not measured or observed.

8 **Response:** We are grateful for the comment. We admit that key product species of isoprene and
9 RO_x radicals of isoprene were not measured during our observation. Therefore, we changed
10 the title into “Explicit modeling of isoprene chemical processing in polluted air masses in
11 suburban areas of the Yangtze River Delta region: radical cycling and formation of ozone and
12 formaldehyde”

13
14 2) Is DSH a rural site? It is characterized as suburban by Lin et al. (2020) and impacted by a
15 nearby freeway. Lin et al. (2020) indicate that both DSH and PD (urban site) are dominated by
16 vehicle emissions sites (Figure 10) and isoprene emission is less in DSH than PD (Figure 5)?
17 Can analysis be done for these five episodes in this study to demonstrate isoprene dominates
18 among VOCs? Otherwise, it is hard to justify the study objective.

19 **Response:** Thanks for the reviewers’ helpful advice. According to former studies (e.g. Lin et
20 al. (2020)), DSL site is a suburban site. We have corrected our description in the revised
21 manuscript. Under stagnant conditions, typically during early morning, DSL could be affected
22 by nearby vehicle emissions. Figure 5 of Lin et al. (2020) exhibited the relative incremental
23 reactivity (RIR) value of O₃ precursors. In their study, RIR of isoprene is lower at DSH than
24 that at PD site, suggesting that more O₃ could be produced at PD site when a same proportion
25 of isoprene was increased. However, at DSH, the ratio of the RIR from isoprene to RIR from
26 anthropogenic hydrocarbons (AHC) is higher than that at PD site, indicating that as DSL site,

27 isoprene plays a more important role than entire AHC in the secondary formation of O₃. This
28 is consistent with our objective, and we aim to investigate the influence of isoprene chemistry
29 on O₃ formation at YRD region. To roughly estimate the influence of isoprene on atmospheric
30 oxidation capability, we adopted the approach presented in Zhu et al. (2020) to calculate the
31 OH reactivity. The results suggest that isoprene, accounting for ~19% of the total k_{OH}, is the
32 most significant VOC specie in terms of k_{OH}, with an average value of 0.89 ± 0.44 s⁻¹. This
33 illustrates the significant role of isoprene in the photochemistry in suburban area. These
34 descriptions have been added in the revised manuscript (Line 193-198).



35
36 Figure 5 Average relative incremental reactivity (RIR) values of the O₃ precursors NO_x, anthropogenic
37 hydrocarbons (AHCs), biogenic hydrocarbons (NHCs), and CO at (a) the DSH site and (b) the PD site
38 from 11–26 July.(from Lin et al. (2020))

39 3) Model performance (i.e., OBM in this study) should be conducted against observed key
40 species such as ozone, formaldehyde, and NO_x before the model can be confidently used to
41 simulate other key RO_x species such as OH, HO₂, RO, and RO₂ (e.g., Figures 4, 5, 7-8). For
42 instance, simulated local O₃ is shown in Figure 7(A) but correlative discussion with observed
43 O₃ profile is needed. Similarly, simulated HCHO concentration in Figure 8(A) should be
44 correlated with observed HCHO concentration. Without solid performance evaluation,
45 simulated RO_x radicals are questionable although they are comparable to other literature values,
46 as indicated in this study.

47 Response: We agree that solid performance evaluation is essential. Therefore, comparison of
48 simulated and observed O₃ and HCHO concentration are given in the supporting information.
49 The discussion of simulated and observed O₃ and HCHO concentrations are given in Line 153
50 to Line 164:

51 ”The index of agreement (IOA), mean bias (MB) and normalized mean bias (NMB) are
52 frequently used for model performance evaluation. These three parameters are calculated by
53 Equation (2) to (4), where S_i , O_i , and \bar{O} are the simulated, observed, and average value of the
54 target compound. In this study, the IOA, MB and NMB of O₃ was 0.90, 0.76 and 10%,
55 respectively, suggesting that the model can reasonably reproduce the variations of O₃ and could
56 be used for further analysis. As for HCHO, the IOA, MB, and NMB was 0.74, 2.43, and 48%,
57 respectively. In general, the model overestimated HCHO concentration, especially on July 29
58 and July 30. According to previous studies, the inconsistency between simulated and observed
59 HCHO could be caused by the uncertainties in the treatment of dry deposition, faster vertical
60 transport, uptake of HCHO, and fresh emission of precursor VOCs (Li et al., 2014).
61 Nevertheless, these results still provide valuable information of secondary formation of HCHO
62 at suburban area.”.

63 The NO_x concentrations are constrained by the observed value in our setup, so there is no need
64 to compare the simulated and observed NO_x concentration.

65 Reference:

66 Li, X., Rohrer, F., Brauers, T., Hofzumahaus, A., Lu, K., Shao, M., Zhang, Y. H., and Wahner,
67 A.: Modeling of HCHO and CHOCHO at a semi-rural site in southern China during the
68 PRIDE-PRD2006 campaign, *Atmospheric Chemistry and Physics*, 14, 12291-12305,
69 10.5194/acp-14-12291-2014, 2014.

70

71 4) As mention above, RO_x radicals and key products (i.e., MACR and MVK) photochemically
72 produced by isoprene and other precursors were not measured so model performance couldn't
73 be conducted against these species. Without the validation, this is hard to evaluate the simulated
74 RO_x radicals with confidence, as mentioned above. In addition, over 50 VOCs were measured
75 but they were not utilized in this study. As an example, some VOCs primarily react with OH
76 radical so those VOCs can be used as surrogates to estimate concentration of OH radicals,
77 which can then be compared to simulated OH radicals. For example, Lin et al (2020) used X/E
78 to estimate OH. Another analysis of VOC data can be conducted to evaluate the relative
79 importance of isoprene in total VOCs. Isoprene has to be a significant part of VOCs emissions
80 in order to achieve the objective of this study, evaluating isoprene's importance in rural areas.

81 Response: Thank for the helpful advice. The average regional OH concentration (8.39 ± 5.11
82 $\times 10^6$ molecules cm^{-3}) was estimated by E/X ratio, and relevant descriptions have been added
83 in the revised manuscript. Please refer to Page 10, Line 228-233:

84 "To verify the performance of OBM model, regional mixing ratios of OH during daytime were
85 also calculated by a parameterization method using ratios of measured ethylbenzene and m,p-
86 xylene concentrations (see Text S2). The calculated average regional concentrations of OH
87 ($8.39 \pm 5.11 \times 10^6$ molecules cm^{-3}) was in the same order of the magnitude of the OBM-
88 simulated result ($4.59 \pm 5.11 \times 10^6$ molecules cm^{-3}), suggesting that the OBM-simulated radical
89 concentration is reliable."

90 In addition, the OH reactivity (k_{OH}) from VOCs was calculated and the result shows that
91 isoprene alone can accounted for 19% of the total k_{OH} , indicating the significant role of isoprene
92 in suburban area. Please refer to Page 10, Line 194-199:

93 "To roughly estimate the influence of isoprene on atmospheric oxidation capability, we adopted
94 the approach given in the study of Zhu et al. (2020a) to calculate the OH reactivity (k_{OH}). The
95 result suggested that isoprene, accounting for ~19% of the total k_{OH} , was the most significant

96 VOC specie from the perspective of k_{OH} , with an average value of $0.89 \pm 0.44 \text{ s}^{-1}$. This indicates
97 the significant role of isoprene in the photochemistry in suburban area.”

98 Reference:

99 Zhu, J., Cheng, H., Peng, J., Zeng, P., Wang, Z., Lyu, X., and Guo, H.: O₃ photochemistry on
100 O₃ episode days and non-O₃ episode days in Wuhan, Central China, Atmospheric Environment,
101 223, 10.1016/j.atmosenv.2019.117236, 2020a

102

103 5) Measurements of VOCs are described in detail (Lines 116-125) but VOC analysis is lacking.
104 Additional analysis would be useful. For instance, several types of VOCs (e.g., alkenes and
105 aromatics) contribute to OVOC, an important specie focused in this study (in Figures 6 and 9),
106 so their relationship to OVOC can be evaluated, in addition to the VOC analyses suggested
107 above.

108 Response: Thanks for the reviewer’s helpful advice. Analysis about VOCs and the relationship
109 between VOCs and OVOCs are added in the revised manuscript. Please refer to Line 194-214:
110 ” To roughly estimate the influence of isoprene on atmospheric oxidation capability, we
111 adopted the approach presented in Zhu et al. (2020) to calculate the OH reactivity (k_{OH}). The
112 results suggest that isoprene, accounting for ~19% of the total k_{OH} , is the most significant VOC
113 species in terms of k_{OH} , with an average value of $0.89 \pm 0.44 \text{ s}^{-1}$. This illustrates the significant
114 role of isoprene in the photochemistry in suburban area. Based on the explicit calculation, the
115 total concentration of OVOC was obtained. Due to the complexity of OVOC formation, which
116 involves hundreds of precursors for just one OVOC species, and the complicated chain
117 reactions converting VOCs to OVOCs, it is difficult to give the accurate relationship between
118 VOCs to OVOCs. Since VOCs were mainly oxidized by OH and O₃ during daytime, we applied
119 multi-linear regression model (given in Eq.(5)) to provide the roughly relationship between
120 VOCs and simulated OVOCs.

$$[OVOC] = \beta_0 + \beta_1[Alkane] + \beta_2[Alkene] + \beta_3[Aromatic] + \beta_4[OH] + \beta_5[O_3] \quad (1)$$

121

122 where $\beta_0, \beta_1, \beta_2, \beta_3, \beta_4$, and β_5 are the coefficient from linear regression, [OVOC] and [OH]
123 are the simulated concentration of OVOC and OH, respectively; [Alkane], [Alkene],
124 [Aromatic], [O₃] are the observed concentration of alkane, alkene, aromatic, and O₃. The Sig
125 value and statistical reliability criteria (R) was 0.000 and 0.853 (shown in Table S3),
126 respectively, indicating that the linear relationship represented by the equations (5) is
127 statistically reliable. The $\beta_1, \beta_2, \beta_3$ was 0.027, 0.623, and 0.820, respectively, suggesting that
128 alkenes and aromatics are significant for the simulated OVOC concentration.”

129

130 Technical comments:

131 1) Table 1: SO₂ is listed as one of the measured pollutants but it is not used in this study at all.

132 Please remove it from the table. CO is not listed here but shown in Figure 2.

133 Response: We are grateful for this comment. The description of SO₂ monitoring has been
134 removed from table 1 and CO monitor has been added in table 1.

135

136 2) Figure 2: CO concentration is almost flat so indicates this site is less impacted by traffic-
137 related emissions. This contradicts with Lin et al (2020)’s observation (Figure 3), where NO_x
138 concentrations show traffic related variation in DSH.

139 Response: Thanks for the reviewer’s careful comment. We agree that the CO concentration
140 was almost flat during the scenarios, but when we look at the variation of NO, clearly peaks of
141 NO was found during early morning, which is closed relate to traffic emission, and this result
142 is also consistent with the observation of Lin et al. (2020), which also found clearly morning
143 peak in DSL.

144

145 3) Section 3.3 (line 210+): there is no discussion or description of Figure 5(B).

146 Response: Thanks for the suggestion. Description of Figure 5 has been added in Line 386-
147 390:“To investigate the underlying causes, we calculated the production rate of RO_x (P(RO_x))
148 and loss rate of RO_x (L(RO_x)) in S1, respectively (Figure 5 (B)). From the comparison, we
149 found most of the reaction rates in P(RO_x) and L(RO_x) showed a decrease trend in S1,
150 suggesting that the absence of isoprene slows down the RO_x recycling.”

151

152 4) Figure 8: Net HCHO rate is negative for several hours around noon. What does that mean?
153 Some discussion is needed.

154 Response: The negative net HCHO rate around noon means the net reduction of HCHO.
155 Relative description is given in Line 364-369:”Between 13:00 and 14:00, a negative net(HCHO)
156 was found. Although the reaction of RO+O₂ quickly produced HCHO at afternoon, the
157 depletion pathways, especially the photolysis of HCHO, became more competitive, leading to
158 the net reduction of HCHO. This also indicated that strong photochemical reactions do not
159 monotonously profit the accumulation of HCHO, it can also constrain high HCHO levels in
160 certain situations.”

161

162 5) Figures 6 and 9: It seems the red lines indicate photolysis production of RO_x radicals while
163 blue lines destruction or sink of these radicals. What does the black line represent? Some
164 description is needed.

165 Response: Thanks for this good suggestion. The black lines represent the processes in RO_x
166 recycling, and NO_x recycling, and relative descriptions has been added for Figure 6 and Figure
167 9.

168

169 Minor comments:

170 1) Line 184: should be “series”, not “serious”

171 [Response: We have recorrected this mistake as suggested.](#)

172

173 2) Lines 512 and 517: these two references seem identical.

174 [Response: We have removed the replicated reference.](#)

175

176 3) Term “loss” is used in Figure 5 and its associated text while “destruction” or “sink” in
177 Figures 7 and 8 and their description. They probably meant the same thing but consistency is
178 preferred.

179 [Response: Thanks for the helpful suggestion, the term “loss”, “destruction” and “sink” has been
180 unified in our manuscript.](#)

181

182 4) Line 205: “by separate the formation of RO₂” should be revised for clarity. Do you mean
183 “by separation from the formation of RO₂”?

184 [Response: Thanks for the reviewer’s suggestion, we have changed this sentence into “By
185 separating the formation pathways of RO₂”.](#)

186

187 5) Line 263-264, the last sentence should be “Primary RO_x sources and sinks are in red and
188 blue, respectively.”

189 [Response: We have revised this sentence as suggested.](#)

190

191 Revised manuscript

192 **Explicit modelling of isoprene chemical processing in polluted air**
193 **masses in suburban areas of the Yangtze River Delta region:**
194 **radical cycling and formation of ozone and formaldehyde**
195

196 **Kun Zhang^{a, b}, Ling Huang^{a, b}, Qing Li^{a, b}, Juntao Huo^c, Yusen Duan^c, Yuhang Wang^d, Yangjun**
197 **Wang^{a, b}, Qingyan Fu^c, Li Li^{a, b*}**

198 ^a School of Environmental and Chemical Engineering, Shanghai University, Shanghai, 200444, China

199 ^b Key Laboratory of Organic Compound Pollution Control Engineering, Shanghai University, Shanghai,
200 200444, China

201 ^c Shanghai Environmental Monitoring Center, Shanghai, 200235, China

202 ^d School of Earth and Atmospheric Sciences, Georgia Institute of Technology, Atlanta, GA, USA

203 *Correspondence to* Li Li (Lily@shu.edu.cn)

204

205 **Abstract**

206 Ozone pollution has become one of the most severe environmental problems in China in
207 recent years. Our online observations showed that high **levels** of O₃ were **frequently** observed
208 in **suburban** areas of the Yangtze River Delta (YRD) region even there was no obvious ozone
209 transport from the urban regions. To better understand the formation mechanism of local O₃
210 pollution and investigate the potential role of isoprene chemistry in the budgets of RO_x
211 (OH+HO₂+RO₂) radicals, synchronous observations of volatile organic compounds (VOCs),
212 formaldehyde (HCHO) and meteorological parameters were conducted at a **suburban** site of
213 the YRD region in 2018. Five episodes with elevated O₃ concentrations under stagnant
214 meteorological conditions were identified; an observation-based model (OBM) with the Master
215 Chemical Mechanism was applied to analyze the photochemical processes in these high-O₃
216 episodes. High levels of O₃, nitrogen oxides (NO_x), and VOCs facilitated strong production

217 and recycling of RO_x radicals with the photolysis of oxygenated VOCs (OVOCs) being the
218 primary source. Our results suggest that local biogenic isoprene is important to suburban
219 photochemical processes. Removing isoprene could drastically slow down the efficiency of
220 RO_x recycling and reduce the concentrations of RO_x. The absence of isoprene chemistry could
221 further lead to decrease in the daily average concentration of O₃ and HCHO by 34% and 36%,
222 respectively. This study underlines that the isoprene chemistry in suburban atmosphere
223 becomes important with the participation of anthropogenic NO_x and also provides insights into
224 the radical chemistry that essentially drives the formation of secondary pollutants (e.g. O₃ and
225 HCHO) in suburban YRD region.

226 **Keywords:** Isoprene; Observation-based model (OBM); Radical; Ozone; Yangtze River Delta

227 1. Introduction

228 The hydroxyl radical (OH), hydro peroxy radical (HO₂) and organic peroxy radical (RO₂),
229 collectively known as RO_x dominate the oxidative capacity of the atmosphere and hence
230 govern the removal of primary contaminants (e.g. volatile organic compounds (VOCs)) and
231 the formation of secondary pollutants (e.g. ozone (O₃), secondary organic aerosols (SOAs))
232 (Liu et al., 2012;Xue et al., 2016). RO_x radicals can undergo efficient recycling (e.g. OH→
233 RO₂→RO→HO₂→OH) and produce O₃ and oxygenated VOCs (OVOCs) (Liu et al., 2012;Tan
234 et al., 2019;Xue et al., 2016). In addition, the photolysis of OVOCs can in turn produce primary
235 RO₂ and HO₂ radicals, and further accelerate the recycling of RO_x (Liu et al., 2012). The
236 reaction rates of different VOCs with RO_x vary significantly (Atkinson and Arey, 2003;
237 Atkinson et al., 2006). For instance, the reaction rate constants for OH with ethane and ethene
238 are 0.248×10^{-12} (cm molecule⁻¹ s⁻¹) and 8.52×10^{-12} (cm molecule⁻¹ s⁻¹), respectively. Among
239 the hundreds thousands of VOC species, isoprene (C₅H₈, 2-methyl-1,3-butadiene) is one of the
240 most active species, and also the most abundant biogenic VOCs (BVOCs) species globally

241 (Wennberg et al., 2018). Isoprene emissions from biogenic sources have been extensively
242 studied over past decades (Gong et al., 2018) and recent works have switched from emissions
243 to the degradation pathways and the impact of isoprene chemistry on regional forest chemistry
244 (Gong et al., 2018; Wolfe et al., 2016a). Previous studies showed that isoprene could be quickly
245 oxidized by atmospheric oxidants (e.g. OH, O₃ or NO₃) (Wolfe et al., 2016a; Gong et al., 2018;
246 Jenkin et al., 2015). Due to the rapid reaction between OH and isoprene ($100 \times 10^{-12} \text{ cm}^3$
247 $\text{molecule}^{-1} \text{ s}^{-1}$ at 298 K), more than 90% of the total daytime isoprene is removed via this
248 reaction (Wennberg et al., 2018). The reaction between OH and isoprene is initiated by the
249 addition of OH and can generate isoprene hydroxyperoxy radicals (ISOPO₂) (Wennberg et al.,
250 2018; D'Ambro et al., 2017; Liu et al., 2013; Jenkin et al., 2015). ISOPO₂ isomers could then
251 interconvert rapidly due to reversible O₂ addition and are finally removed via reactions with
252 HO₂ or NO (Jenkin et al., 2015; Wolfe et al., 2016a). Hence, the degradation process of
253 isoprene is tightly associated with RO_x recycling. According to He et al. (2019), isoprene
254 chemistry could strongly influence the photochemical formation of O₃, with a relative
255 incremental reactivity (RIR) of ~0.06%/%. In addition to O₃, HCHO is formed via several
256 pathways during the depletion of isoprene (Jenkin et al., 2015; Wolfe et al., 2016a) and HCHO
257 formation is found to be highly sensitive to isoprene (Zeng et al., 2019).

258 The Yangtze River Delta (YRD) region is one of the most developed city-clusters in
259 eastern China and has been suffering from serious O₃ pollution (Zhang et al., 2019; Zhang et
260 al., 2020a; Chan et al., 2017). At the suburban area of YRD, high levels of O₃ were frequently
261 observed (Zhang et al., 2019; Zhang et al., 2020a). A number of studies have been conducted
262 to investigate the relationships between O₃ precursors and O₃ (Chan et al., 2017; Lin et al.,
263 2020; Zhang et al., 2020a; Zhang et al., 2020b), but few have attempted to address the
264 atmospheric oxidizing capacity and radical chemistry involved in these complicated
265 photochemical processes (Tan et al., 2019; Zhu et al., 2020b). Previous studies have pointed

266 out that high **levels** of O₃ at suburban areas of Shanghai could be attributed to the transport of
267 O₃ or O₃ precursors from urban areas (Lin et al., 2020; Zhang et al., 2019). However, high O₃
268 **concentrations were** frequently observed in suburban areas under stable meteorological
269 conditions. Given the high vegetation coverage in **suburban** YRD and weak transport of air
270 masses, the importance of local isoprene chemistry to ozone formation remains unclear.

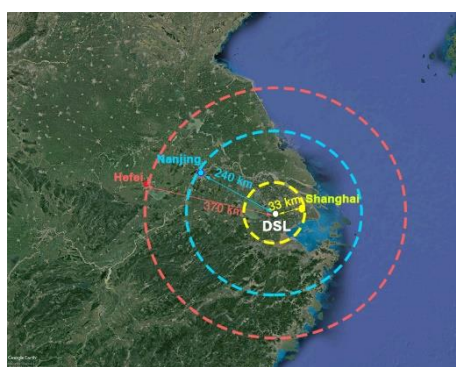
271 In this study, we conducted a comprehensive set of in-situ observations of isoprene,
272 meteorological parameters, and trace gases to understand the **important impact** of isoprene
273 chemistry **on** atmospheric photochemical processes in **suburban** YRD region. An observation-
274 based model (OBM) was used to explore the role of local isoprene chemistry in radical budgets
275 and the formation of O₃ and HCHO. Results from this study can provide insights **into** the
276 isoprene chemistry in the **suburban** region of a fast-developing city-cluster.

277 **2. Methodology**

278 **2.1 Measurement site and techniques**

279 The observations were conducted at a supersite (120.98°E, 31.09°N) in the **suburban** areas
280 of the YRD region (Figure 1). It is located **in** the west of Shanghai and is close to the Dianshan
281 Lake Scenic area, which has high vegetation coverage. To investigate the local isoprene
282 chemistry and its influence on O₃ and HCHO formation, continuous measurements were
283 conducted from Apr. 7 to Sep. 25, 2018, when the photochemical reactions are active and ozone
284 formation is significant.

285



286

287 **Figure 1. Location of the Dianshan lake supersite (white dot) in the suburban areas of YRD region.**

288 **This picture was created with Google Earth© on 23rd July 2020.**

289 **Table 1. Measurements performed during the ozone season**

Species/Parameter	Experimental Technique	Time resolution	Lower Detectable limit
O ₃	Model 49i, Thermo Fischer Scientific, USA	60 s	0.5 ppbv
NO and NO ₂	Model 42i, Thermo Fischer Scientific, USA	60 s	0.4 ppbv
CO	Model 48i, Thermo Fischer Scientific, USA	60 s	40 ppbv
HCHO	AL4021, Aero-Laser, GER	90 s	0.1 ppbv
VOCs species	GC866, Agilent., USA	1 hour	-
Temperature, relative humidity, wind speed and wind direction	Meteorological station, Vaisala, NLD	60 s	-

290

291 The measuring instruments are shown in Table 1. Wind speed (WS), wind direction (WD),
292 temperature (T), and relative humidity (RH) were simultaneously observed by a meteorological
293 station (Vaisala., FIN). According to China's air quality standard, several criteria air pollutants
294 were measured during this experiment. O₃ was measured by an ultraviolet photometric analyzer
295 (Model 49i, Thermo Fischer Scientific., USA), which has a detection limit of 0.5 ppbv at 60
296 second resolution. 1 min resolution of nitrogen oxides (NO and NO₂) data were simultaneously
297 observed by a chemiluminescence instrument (Model 42i, Thermo Fischer Scientific., USA),
298 which has a detection limit of 0.4 ppbv. Carbon monoxide was monitored by a gas filter
299 correlation infrared absorption analyzer (Model 48i, Thermo Fischer Scientific., USA), which
300 has a detection limit of 0.04 ppm. All the online instruments used for gas analyzer were auto-
301 zero every day, and were multi-point calibrated every month. All the instruments used for the
302 online observation were housed on top of a 5-floor-high building, which was about 15 m above
303 the ground level.

304 A total of 55 VOC species, including 28 alkanes, 10 alkenes, 16 aromatics and acetylene
305 were continuously analyzed at our sampling site by two online gas chromatograph with flame
306 ionization detector (GC-FID) systems (GC-866 airmoVOC C₂-C₆ #58850712 and airmoVOC
307 C₆-C₁₂ #283607112, Agilent., USA) with a time resolution of 1 hour during our experiment.

308 Ambient samples are directly inhaled into this system by a pump. Low carbon VOCs (C₂-C₆)
309 are captured by a low temperature (-10 °C) preconcentration system, while high carbon VOCs
310 are concentrated by a built-in room temperature preconcentration system. Then the
311 preconcentration systems are heated and desorb VOCs, which are then carried into
312 chromatographic columns by helium. Individual VOCs separated in the columns are eventually
313 detected by FID systems. Formaldehyde (HCHO) was continuously measured by a Hantzsch
314 fluorescence technique (AL4201, Aerolaser GmbH., GER), which is based on fluorometric
315 Hantzsch reaction in the liquid phase, requiring the quantitative transfer of HCHO from gas
316 phase to liquid phase. A Hantzsch reagent (acetylacetone) was used in this instrument.

317 **2.2 Observation-based model**

318 A user-friendly zero-dimensional (0-D) box model (F0AM) was used to simulate the
319 chemical processes in the atmosphere in this study. This model was developed by Wolfe et
320 al.(2016b) based on University of Washington Chemical Model (UWCM). Dry deposition,
321 aloft exchange, and atmospheric dilution were considered in this model. We chose the Master
322 Chemical Mechanism (MCM) v3.3.1 as the chemical mechanism with more than 5,800
323 chemical species and 17,000 reactions, which enables a detailed description of the complex
324 reactions. In addition to gas-phase reactions, several heterogenous processes including the
325 uptake of HO₂, N₂O₅ and HCHO on aerosol surface, and heterogenous source of HONO were
326 also considered in our simulation. These reactions rate constants and uptake coefficient were
327 obtained from the study of Riedel et al. (2014), Xue et al. (2014) and Li et al. (2014). Since
328 key parameters such as aerosol surface areas (S_A) and particle diameters (r) were not measure
329 during our observation, an average S_A (640 nm²/cm³) was obtained from the field campaign in
330 Shanghai (Wang et al., (2014)).

331 **Table 2. Heterogenous reactions and associated rate constants used in the OBM model**

Reactions	Reaction rate constant	Reference
-----------	------------------------	-----------

$N_2O_5 \rightarrow CLNO_2 + HNO_3$	$\gamma\omega S_A/4$ (for $CLNO_2$ formation)	Riedel et al. (2014)
	$(2 - \phi)\gamma\omega S_A/4$ (for HNO_3 formation)	
$NO_2 \rightarrow HONO$	$k_g = \frac{1}{8} \times \omega \gamma_g \left(\frac{S}{V}\right)$	Xue et al. (2014)
	$k_a = \frac{1}{4} \omega \gamma_a S_A$	
$HO_2 \rightarrow products$	$k = \left(\frac{r}{D_g + \gamma} \omega\right)^{-1} S_A$	Xue et al. (2014)
$HCHO \rightarrow products1$	$k = \frac{1}{4} \omega \gamma S_A$	Li et al. (2014)

γ = uptake coefficient for the given reactant with aerosol surface area; ϕ = product yield; ω =mean molecular speed of the given reactant (m/s); S_A =RH corrected aerosol surface area concentration (nm^2/cm^3); r =surface-weighted particle radius.

332

333 Photolysis frequencies (J values) were calculated by a trigonometric parameterization
 334 based on solar zenith angle (SZA):

$$J = I \cos(SZA)^m \exp(-n \sec(SZA)) \quad (2)$$

335 where I , m and n are constants unique to each photolysis reaction, derived from least-squares
 336 fits to J values computed with fixed solar spectra and literature cross-section and quantum
 337 yields (Wolfe et al., 2016b). Hourly averaged concentrations of speciated VOCs (except
 338 **HCHO**), NO, NO₂, **CO** and meteorological parameters (such as T, RH and P) were used to
 339 constrain the F0AM model. Nitrous acid (HONO) was not measured during our observation.
 340 Therefore, it was fixed as 2% of the observed NO₂ concentration. This constant ratio is well
 341 observed in different field studies and performed well in previous box model studies (Tan et
 342 al., 2019). Before each simulation, the model will run 3 days as spin up to reach a steady state
 343 for unmeasured species (e.g., OH and NO₃ radicals). The comparison of simulated and
 344 observed O₃ and **HCHO** concentrations is shown in Figure S1 and Figure S2. The index of
 345 agreement (IOA), mean bias (MB) and normalized mean bias (NMB) are frequently used to

346 estimate the model performance. These three parameters can be calculated by Equation (3) to
 347 (5), where S_i , O_i , and \bar{O} are the simulated, observed, and average observed value of the target
 348 compound. In this study, the IOA, MB and NMB of O_3 was 0.90, 0.76 and 10%, respectively.
 349 This result suggests that the model can reasonably reproduce the variations of O_3 and could be
 350 used for further analysis. As for HCHO, the IOA, MB, and NMB was 0.74, 2.43 and 48%,
 351 respectively. In general, the model overestimated HCHO concentration, especially on July 29
 352 and July 30. According to previous studies, the inconsistency between simulated and observed
 353 HCHO could be caused by the uncertainties in the treatment of dry deposition, faster vertical
 354 transport, uptake of HCHO, and fresh emissions of VOCs precursors (Li et al., 2014). But the
 355 result still provides valuable information of secondary formation of HCHO at suburban area.
 356 To quantify the atmospheric oxidative capacity (AOC) changes in response to isoprene
 357 chemistry, two parallel scenarios (S0 and S1) were conducted with isoprene chemistry disabled
 358 in S1. In both cases, identical chemical mechanism and meteorological conditions were used
 359 to drive model simulations. Through a comparative analysis of the scenarios, the impact of
 360 isoprene chemistry on AOC and secondary formation of O_3 and HCHO can be obtained.

$$IOA = 1 - \frac{\sum(S_i - O_i)^2}{\sum(|S_i - \bar{O}| + |O_i - \bar{O}|)^2} \quad (3)$$

$$MB = \frac{\sum(S_i - O_i)}{N} \quad (4)$$

$$NMB = \frac{\sum(S_i - O_i)}{\sum O_i} \times 100\% \quad (5)$$

361 **3. Results and discussions**

362 **3.1 Overview of the observations**

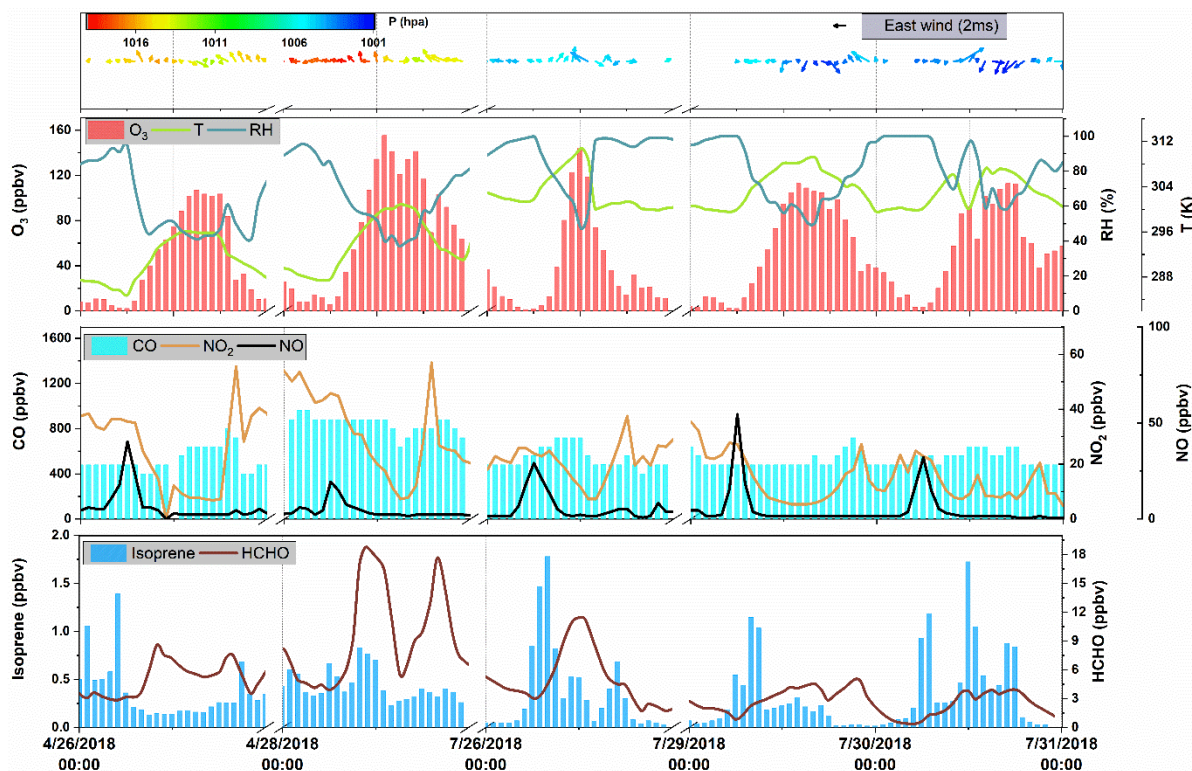
363 To investigate the impact of local chemistry on ozone formation, five days with low daily
 364 average wind speed (<2m/s) and high maximum daily 8-h average (MDA8) O_3 concentration
 365 (>74.7 ppb) were identified as typical local chemistry cases. Figure 2 shows the time series of

366 observed meteorological parameters (P, T, and RH), trace gases (NO, NO₂ and O₃), isoprene
367 and HCHO on selected days. During those episodes, the air masses reaching the site were
368 mainly from southeast and southwest (Figure 2). The weak wind was not conducive to the
369 regional transportation of air pollutants. The observed O₃, NO₂, NO, CO, and TVOC ranged
370 from 1.40 to 155.40 ppbv (52.72 ± 44.43 ppbv, average value, the same below), 5.36 to 57.95
371 ppbv (21.58 ± 12.88 ppbv), 0.75 to 54.51 ppbv (5.40 ± 8.13 ppbv), 400 to 960 ppbv (597 ± 153
372 ppbv), and 2.34 to 20.33 ppbv (7.28 ± 4.32 ppbv) respectively. During the five episodes, the
373 average concentrations of alkanes, alkenes, and aromatics were 13.97 ± 9.12 , 3.27 ± 2.31 , and
374 4.93 ± 2.69 ppbv, which were about 53%, 18%, and 50% higher than of the whole observation.
375 The conditional probability function (CPF) is applied to exhibit the relationship between high
376 O₃ concentrations and wind (Figure 3). The detailed description of CPF can be found in
377 supplemental information (Text S1). The result suggests that high O₃ concentrations (>131 ppb)
378 was usually observed when the site was influenced by weak south wind. This implies that high
379 O₃ was most likely formed locally. Although this site is far away from urban areas, high levels
380 of NO were found during early morning, which is likely caused by nearby fresh emissions. As
381 for NO₂, only one peak was found at dusk. This was different from the results in urban areas
382 (Zhang et al., 2019). It is worth noting that NO₂ and O₃ concentrations were high even during
383 nighttime, suggesting that the AOC remained high at nighttime. The daily average isoprene
384 concentrations were 0.37 ± 0.36 ppbv, which is comparable to that observed by Gong et al.
385 (2018) at a forested mountaintop site (0.287 ± 0.032 ppbv). To roughly estimate the influence
386 of isoprene on atmospheric oxidation capability, we adopted the approach given in the study
387 of Zhu et al. (2020a) to calculate the OH reactivity (k_{OH}). The result suggested that isoprene,
388 accounting for ~19% of the total k_{OH} , was the most significant VOC specie from the perspective
389 of k_{OH} , with an average value of 0.89 ± 0.44 s⁻¹. This indicates the significant role of isoprene
390 in the photochemistry in suburban area. The average HCHO was 5.01 ± 3.80 ppbv, which was

391 ~2 times of that observed at a rural site of Hong Kong (Yang et al., 2020). It is worth noting
392 that HCHO could reach 18.69 ppbv at midday. Based on the explicit calculation, the total
393 concentration of OVOC was obtained. Due to the complexity of OVOC formation, which could
394 have hundreds of precursors for just one OVOC specie, and the complicated chain reactions
395 converting VOCs to OVOCs, it is difficult to give the accurate relationship between VOCs to
396 OVOCs. Since VOCs were mainly oxidized by OH and O₃ during daytime, in this study, we
397 chose multi-linear regression model (given in Eq.(6)) to explore the roughly relationship
398 between VOCs and simulated OVOCs.

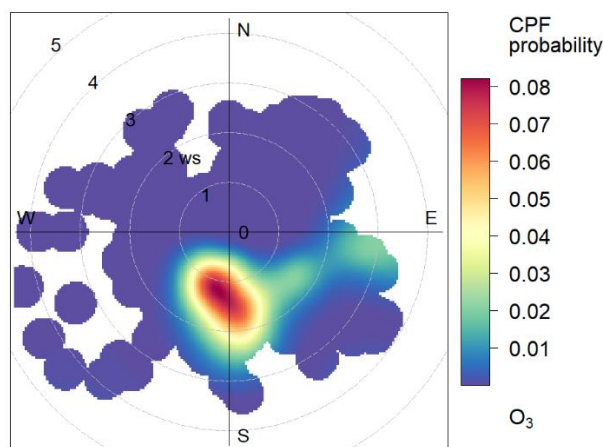
$$[OVOC] = \beta_0 + \beta_1[Alkane] + \beta_2[Alkene] + \beta_3[Aromatic] + \beta_4[OH] + \beta_5[O_3] \quad (6)$$

399 where β_0 , β_1 , β_2 , β_3 , β_4 , and β_5 are the coefficient from linear regression; [OVOC] and [OH] are
400 the simulated concentration of OVOC and OH, respectively; [Alkane], [Alkene], [Aromatic],
401 [O₃] are the observed concentration of alkanes, alkenes, aromatics, and O₃, respectively. The
402 Sig value and statistical reliability criteria (R) was 0.000 and 0.853 (shown in Table S2),
403 respectively, indicating that the linear relationship represented by equations (6) is statistically
404 reliable. The β_1 , β_2 , β_3 was 0.027, 0.623, and 0.820, respectively, suggesting that alkenes and
405 aromatics are significant for the simulated OVOC concentration.



406
407
408

Figure 2. Time series of hourly averages for trace gases, isoprene, HCHO, and meteorological parameters.



CPF at the 95th percentile (=131)

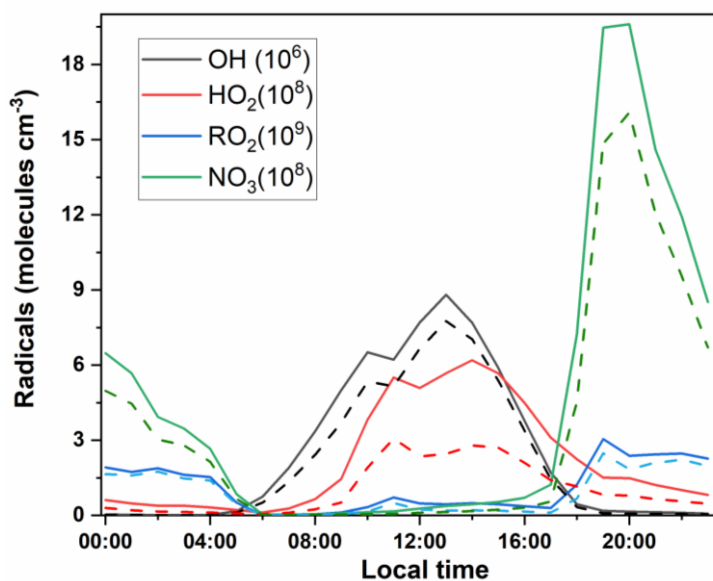
409
410

Figure 3. CPF polar plot of O₃ at DSL station.

411 3.2 Simulated concentrations of radicals

412 Figure 4 shows the simulated average diurnal variation of major radicals in the base
413 scenario (S0). The average concentrations of OH, HO₂, RO₂, and NO₃ were estimated at 2.11
414 $\times 10^6$, 1.04×10^8 , 0.90×10^9 , and 3.49×10^8 molecules cm⁻³, respectively. The simulated daily

415 average OH concentration lies between the simulated values during the summer in Beijing (9
416 $\times 10^6$ molecules cm^{-3}) and the simulated value at a suburban site in Hong Kong in 2013 ($1.5 \pm$
417 0.2×10^6 molecules cm^{-3}) (Liu et al., 2019; Xue et al., 2016). In addition, the average simulated
418 daytime OH concentration was $\sim 50\%$ lower than that simulated at a forested mountaintop site
419 in southern China (Gong et al., 2018). To verify the performance of OBM model, regional
420 mixing ratios of OH during daytime were also calculated by a parameterization method using
421 measured ethylbenzene and *m,p*-xylene ratios (see Text S2). The calculated average regional
422 concentrations of OH ($8.39 \pm 5.11 \times 10^6$ molecules cm^{-3}) was in the same magnitude of the
423 OBM-simulated result ($4.59 \pm 5.11 \times 10^6$ molecules cm^{-3}), suggesting that the OBM-simulated
424 radical concentration is reliable. The maximum HO₂ concentration simulated for DSL site (6.19
425 $\times 10^8$ molecules cm^{-3}) was close to that reported in Beijing (6.8×10^8 molecules cm^{-3}) (Liu et
426 al., 2012), but was $\sim 32\%$ higher than that in Wuhan (4.7×10^8 molecules cm^{-3}) (Zhu et al.,
427 2020a). Pretty high levels of simulated NO₃ (as high as $\sim 19 \times 10^8$ molecules cm^{-3}) was found
428 during nighttime. The average simulated nocturnal NO₃ concentration was 8.80×10^8 molecule
429 cm^{-3} , which was $\sim 47\%$ higher than that simulated in the study of Gong et al.(2018). As
430 aforementioned, during nighttime, pretty high levels of NO₂ (27.71 ppbv) and O₃ (30.05 ppbv)
431 was observed, which favored the formation of NO₃. Interestingly, a high level of RO₂ was also
432 found during nighttime. This result is different from the study of Liu et al. (2012), which found
433 the maximum value of RO₂ during daytime. By separating the formation pathways of RO₂, we
434 found that during nighttime, over 70% RO₂ was produced via the oxidation of VOCs by NO₃
435 radical, suggesting that the nighttime chemistry in the suburban site was also very important.
436



437
438 **Figure 4. Simulated average** diurnal variation of OH, HO₂, RO₂ and NO₃ in S0 (solid lines) and S1
439 (dash lines).

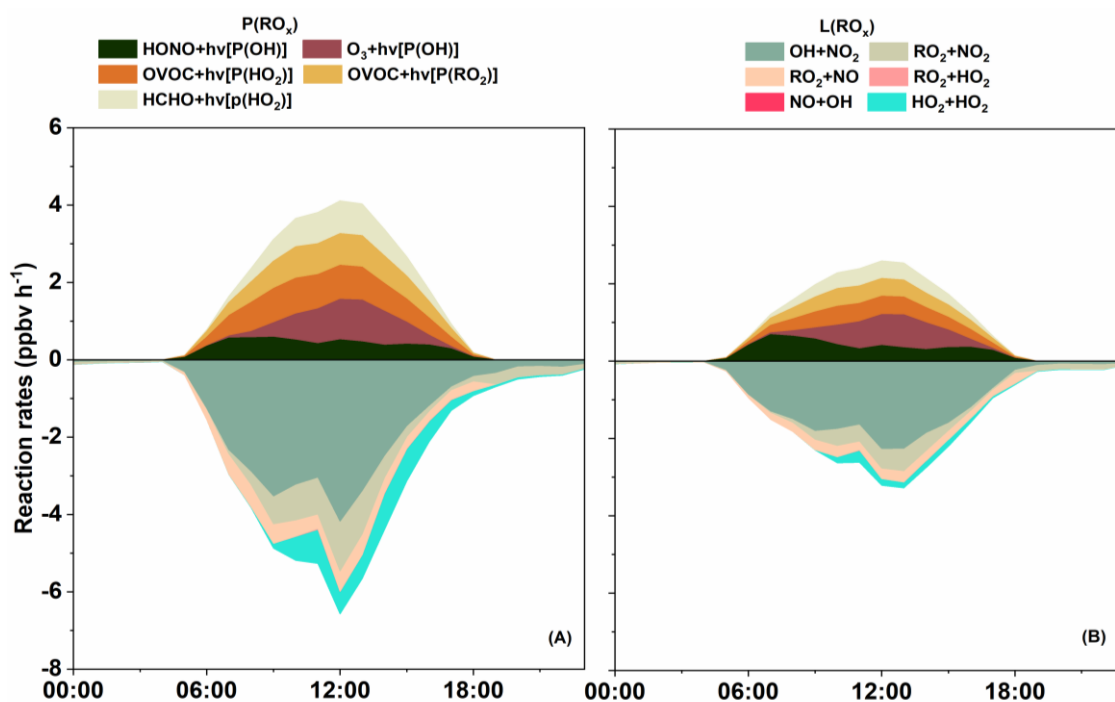
440 3.3 Recycling of RO_x radicals

441 Figure 5(A) shows the primary sources of RO_x in S0 and the detailed daytime budget of
442 RO_x. Minor RO_x sources, e.g. **ozonolysis** of alkenes, are not shown. The photolysis of O₃ **was**
443 the predominant primary source of OH, with a daytime mean production rate of **0.50** ppbv h⁻¹,
444 which was comparable to that found by Liu et al. (2012) in Beijing, but was **0.40** ppbv h⁻¹ lower
445 than the result in the study of Xue et al. (2016). **Another important OH source is the** photolysis
446 of HONO, contributing **0.32** ppbv h⁻¹ of daytime OH production in our simulation. This value
447 is much lower than the results of Liu et al. (2019) and Xue et al. (2016). Such low value was
448 most likely caused by the excessive constrain on HONO since HONO was not directly
449 monitored during our experiment. **Sensitive studies were conducted to quantify the influence**
450 **different of HONO/NO₂ ratio on radical recycling (Text S3, Figure. S1 and Table S1). As**
451 **expected, a lower HONO/NO₂ ratio leads to a lower HONO concentration, and subsequent less**
452 **OH reduce generated from the photolysis of HONO. The sensitive studies show that when**
453 **HONO/NO₂ ratio is 0.005, the daytime OH level could decrease by 15.28%. Vice versa, a**
454 **higher HONO/NO₂ (e.g., 0.04) can promote OH concentration by 14.08%. This result indicates**

455 that the photolysis of HONO is essential to the generation of OH, and therefore a simultaneous
456 measurement of HONO is highly recommended for the analysis of local radical recycling in
457 the future. As for HO₂, the photolysis of OVOC (excluding HCHO) is the predominant source
458 with a daytime mean production rate of 0.65 ppbv h⁻¹ and maximum reaching 0.92 ppbv h⁻¹,
459 which is comparable to Xue et al. (2016). The photolysis of HCHO can also contribute 0.48
460 ppbv h⁻¹ to the daytime production of HO₂, which is close to the results of Xue et al. (2016).
461 As for RO₂, the photolysis of OVOC was the largest source (0.57 ppbv h⁻¹), which was
462 relatively lower than the results found at urban site (Liu et al., 2012). From the RO_x perspective,
463 the daytime primary radical production in DSL site was dominated by the photolysis of OVOC
464 (except for HCHO), followed by the photolysis of HCHO and O₃. But the photolysis of HONO
465 can become the overriding RO_x source around run rising, which suggests that HONO can be
466 an important OH reservoir species during nighttime. Summing up all the sources of RO_x gives
467 a total primary daytime RO_x production rate of 2.55 ppbv h⁻¹ (0.84 ppbv h⁻¹ for OH, 1.14 ppbv
468 h⁻¹ for HO₂, and 0.57 ppbv h⁻¹ for RO₂), which was 61~69% lower than those in Beijing (6.6
469 ppbv h⁻¹, Liu et al. (2012)) and Hong Kong (8.11 ppbv h⁻¹, Xue et al. (2016)), indicating that
470 the recycling of RO_x in Beijing and Hong Kong could be much reactive.

471 RO_x radicals are ultimately removed from the atmosphere via deposition of radical reservoir
472 species, e.g. H₂O₂, HNO₃, and ROOH (Liu et al., 2012). The terminate processes of RO_x was
473 dominated by their reactions with NO_x. Specifically, the reaction of OH+NO₂, RO₂+NO₂,
474 RO₂+NO, forming HNO₃, RO₂NO₂, and RONO₂, accounting for 2.42, 0.56, and 0.41 ppbv h⁻¹
475 of the RO_x radical sink during daytime. This is consistent with the understanding that reactions
476 with NO_x usually dominate the radical sink in high NO_x environments (Xue et al., 2016; Liu
477 et al., 2012). In addition, RONO₂ and RO₂NO₂ could in turn react with OH, leading to 0.41
478 ppbv h⁻¹ of daytime OH sinks (Figure 6). Summing up the primary sources and sinks gives a

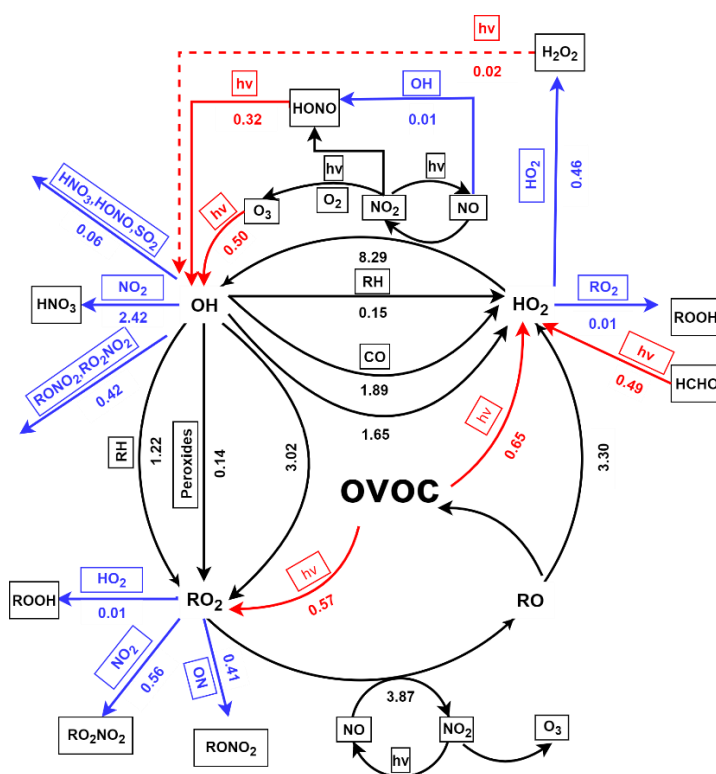
479 negative value of net RO_x production, suggesting that the RO_x was in a stage of gradual
 480 depletion.



481
 482 **Figure 5. Simulated primary daytime sources and sink of RO_x in S0 (A) and S1 (B).**

483 The daytime (6:00-18:00) average budget of RO_x is shown in Figure 6, with primary
 484 sources of RO_x in red, sinks of RO_x in blue, and recycling processes in black. In the recycling
 485 of RO_x, the production of OH was dominated by the reaction of HO₂+NO (8.29 ppbv h⁻¹). As
 486 for RO₂, it was produced by the reaction of OH with OVOC (3.02 ppbv h⁻¹), alkyl (RH) (1.21
 487 ppbv h⁻¹), and peroxides (0.14 ppbv h⁻¹). The reaction of RO₂+NO can result in strong
 488 production of RO (3.87 ppbv h⁻¹). The reaction of RO and O₂ was the major contributor to
 489 HO₂ production, followed by the reaction of OH with CO (1.89 ppbv h⁻¹), OVOC (1.59 ppbv
 490 h⁻¹), and RH (0.15 ppbv h⁻¹). It should be noted that the top two fast reactions within the
 491 recycling of RO_x (HO₂+NO and RO₂+NO) were related to NO_x. As mentioned in the study
 492 of Liu et al. (2012), this result could be mainly due to the abundance of NO (e.g. ~50 ppbv in
 493 the morning). Obviously, these recycling processes dominate the total production of OH, HO₂
 494 and RO₂ radicals. As suggested in the study of Xue et al. (2016) and Liu et al. (2012), the

495 radical propagation is efficient and enhances the effect of the newly produced radicals in the
 496 polluted atmospheres with the co-existence of abundant NO_x and VOCs.

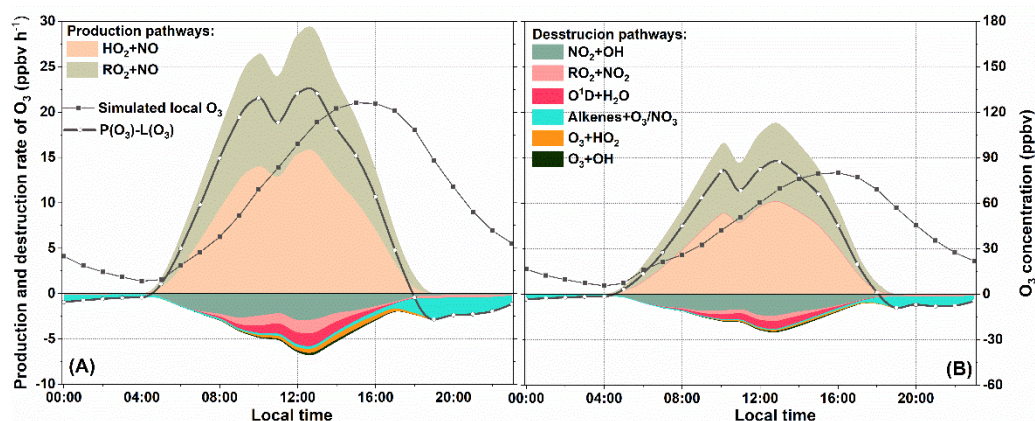


497
 498 **Figure 6. Summary of daytime (06:00-18:00) average budgets of RO_x radicals (in ppbv h⁻¹).**
 499 **Primary RO_x sources and sinks are in red and blue, respectively, and the black lines represent the**
 500 **processes in RO_x and NO_x recycling.**

501 3.4 Formation and sink of O₃

502 Figure 7 illustrates the diurnal variation of simulated O₃ formation and sink pathways in
 503 S0. Also shown is the simulated average diurnal pattern of O₃ concentration and the net O₃
 504 production rate. In the troposphere, the formation of O₃ is via the reactions of NO with peroxy
 505 radicals (e.g. HO₂ and RO₂) (Liu et al., 2012; Xue et al., 2016; Zhu et al., 2020a). On average,
 506 the reaction of HO₂+NO and RO₂+NO attributed 5.05 and 4.62 ppbv h⁻¹ of the production of
 507 O₃. The maximum rate of HO₂+NO (15.36 ppbv h⁻¹) and RO₂+NO (13.26 ppbv h⁻¹) both
 508 occurred at 13:00. The total daytime production rate of O₃ (P(O₃)) is the sum of HO₂+NO and
 509 RO₂+NO at 17.86 ppbv h⁻¹, which lies between that simulated in Beijing (32 ppbv h⁻¹, Liu et
 510 al. (2012)) and Hong Kong (6.7 ppbv h⁻¹, Liu et al. (2019)). Due to the fast cycling of both O₃

511 and NO₂, the sink of O₃ was due to several reactions leading to the destruction of O₃ and NO₂.
 512 In our cases, the reaction of NO₂+OH becomes the predominant scavenging pathways of O₃,
 513 with an average daytime reaction rate of 1.89 ppbv h⁻¹ (49%, percentage of the total O₃ sink
 514 rate, same below). This is comparable to the study of Liu et al. (2012 and 2019). The reaction
 515 of RO₂+NO₂ was the second contributor to O₃ sink, with a mean contribution of 0.62 ppbv h⁻¹
 516 (16%). Other pathways, e.g. photolysis of O₃, ozonolysis of alkenes, and O₃+HO₂, together
 517 contributed 1.11 ppbv h⁻¹ of the total sink rate of O₃ during daytime. The daytime mean L(O₃)
 518 was 3.87 ppbv h⁻¹, which was ~22% of P(O₃), suggesting that O₃ could efficiently accumulate
 519 during daytime. The net production of O₃ (P(O₃)-L(O₃)) is also shown in Figure 7. The
 520 maximum O₃ concentration was found at around 16:00, which was also observed in other
 521 suburban sites (Zong et al., 2018; Zhang et al., 2019). It is worth noting that, the reaction of
 522 alkenes+O₃/NO₃ serves as an important pathway of O₃ sink during nighttime (as high as 2.30
 523 ppbv h⁻¹).



524 **Figure 7. Simulated average diurnal profiles of O₃ formation and sink rates (ppbv h⁻¹) in S0 (A) and**
 525 **S1 (B).**

527 3.5 Formation and sink of HCHO

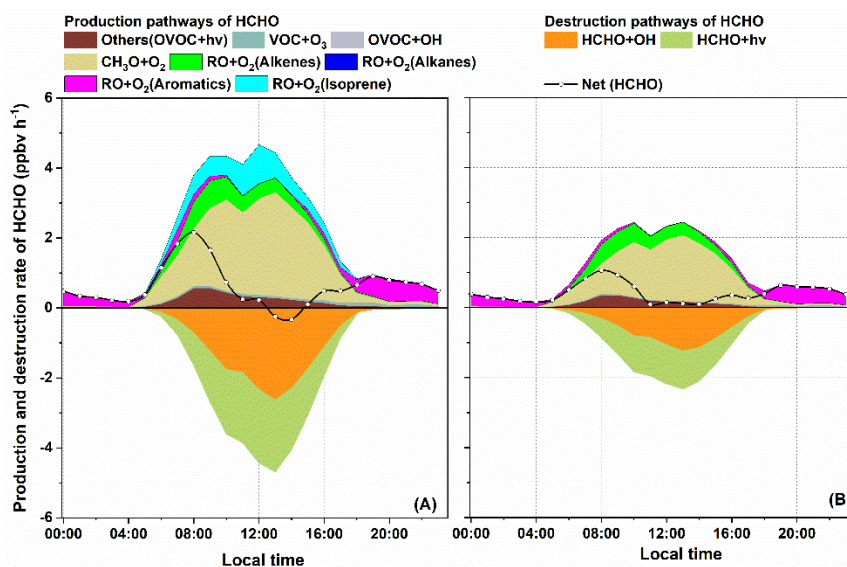
528 As aforementioned, high levels of HCHO was observed at DSL. Figure 8 (A) shows the
 529 production and sink pathways of HCHO in S0. On average, HCHO formation was dominated
 530 by the reaction of RO+O₂, accounting for ~90% of the total production rate. Further

531 classification of RO+O₂ pathway suggested that the oxidation of CH₃O made a significant
532 contribution of ~47%, followed by RO (from isoprene) + O₂ reaction (12%) and RO (from
533 aromatics) + O₂ reaction (~11%). This result is comparable to the study of (Yang et al., 2020;
534 Yang et al., 2018). It is notable that the reaction of RO (from aromatics) + O₂ could become
535 the predominant pathway of HCHO production during nighttime. This could be attributed to
536 the high level of NO₃ during nighttime, by which styrene could be quickly oxidized and
537 generate N-containing RO radicals, and furtherly generate HCHO. During daytime, isoprene
538 became the most important VOC specie of HCHO production, with a mean rate of 0.48 ppbv
539 h⁻¹. As mentioned, this site is surrounded by highly vegetated areas, which can provide
540 abundant biogenic isoprene. During daytime, over 90% of isoprene was oxidized by OH
541 radicals (Figure S4). According to MCMv3.3.1, several RO₂ species (e.g. ISOP34O₂,
542 ISOPDO₂, ISOPCO₂, CISOPAO₂, ISOPAO₂) can be generated during the OH-initiated
543 degradation process of isoprene (Jenkin et al., 2015). With the present of NO, isoprene-
544 originated RO₂ can transfer into RO (e.g. ISOPDO, ISOP34O, ISOPAO). The subsequent
545 degradation processes of isoprene-related RO, especially ISOP34O, ISOPDO, ISOPAO and
546 ISOPBO, are tightly related to the formation of HCHO (Jenkin et al., 2015). Other sources of
547 HCHO, such as the reaction between VOC and O₃, photolysis of OVOC and the reaction of
548 OVOC+OH only contributed minor amount of the total production rate during whole day.

549 As for HCHO depletion, the photolysis of HCHO and the reaction of HCHO+OH was the
550 two dominate pathways, accounting for ~52% and ~48% of the total depletion rate, respectively.
551 The net HCHO production rate (equals to P(HCHO) + L(HCHO)) was also shown in Figure 8.
552 After sunrise, the net production rate of HCHO raised gradually until 8:00, when it reached the
553 maximum rate (1.6 ppbv h⁻¹). This result is comparable to the study of Yang et al. (2018). At
554 around 12:00, the net(HCHO) dropped to ~0 ppbv h⁻¹, that was roughly consistent with our
555 observation, which shows that the HCHO peak occurs at around 12:00. Between 13:00 and

556 14:00, a negative net(HCHO) was found. Although the reaction of RO+O₂ quickly produced
 557 HCHO at afternoon, the depletion pathways, especially the photolysis of HCHO, became more
 558 competitive, leading to the net reduction of HCHO. This also indicated that strong
 559 photochemical reactions do not monotonously profit the accumulation of HCHO, it can also
 560 constrain high HCHO levels in certain situations. After 14:00, the photolysis of HCHO dropped
 561 rapidly and the net depletion of HCHO back to ~0 ppbv h⁻¹ at around 15:00. The daytime net
 562 HCHO production rate was 0.70 ppbv h⁻¹, which was comparable to result of Yang et al. (2018).

563 The above analysis indicates that the photolysis of OVOC, HCHO, O₃ and HONO was
 564 the primary source of RO_x, which offers high oxidizing environment for the degradation of
 565 VOCs. As a typical by-product in the degradation of several VOCs, HCHO can be quickly
 566 formatted during daytime. The insight into detailed photochemical processes shows the
 567 important role of isoprene in the formation of HCHO.



568
 569 **Figure 8. Simulated average diurnal profiles of net rate (net (HCHO)), breakdown HCHO**
 570 **production rate and sink rate (ppbv h⁻¹) in S0 (A) and S1 (B).**

571 3.6 Impacts of isoprene chemistry on photochemistry

572 3.6.1 Impact on RO_x budget

573 As aforementioned, the degradation of isoprene is tightly related to the cycling of RO_x.
 574 To roughly explain the impact of isoprene chemistry on RO_x budget, we carried out a parallel

575 simulation (S1) where isoprene chemistry is disabled (see in Figure 9). The diurnal variation
576 of OH, HO₂, RO₂ and NO₃ in S1 is also shown in Figure 4 (B) which clearly suggests the
577 decline in RO_x and NO₃ without isoprene input. To investigate the underlying causes, we
578 calculated the production rate of RO_x (P(RO_x)) and loss rate of RO_x (L(RO_x)) in S1,
579 respectively (Figure 5 (B)). From the comparison, we found most of the reaction rates in P(RO_x)
580 and L(RO_x) showed a decrease trend in S1, suggesting that the absence of isoprene slows down
581 the RO_x recycling. The photolysis of OVOC (0.67 ppbv h⁻¹) is still the predominant primary
582 source of RO_x. However, without isoprene, the photolysis rate of OVOC decreased by 0.49
583 ppbv h⁻¹. The total production and depletion rate of OH dropped to 6.96 and 7.51 ppbv h⁻¹,
584 respectively. Although the absence of isoprene could reduce the consumption of OH, the OH
585 concentration would be reduced by ~16% compared to S0, suggesting that the amount of OH
586 produced via isoprene chemistry is large enough to compensate for the shift from OH to peroxy
587 radicals in the RO_x family. As for RO₂, the daytime production and sink rate falls to 3.25 and
588 3.34 ppbv h⁻¹, respectively. This means the concentration of RO₂ would be in a stage of gradual
589 decrease. In addition, the absence of isoprene could also reduce RO₂ concentration by ~20%,
590 suggesting that isoprene was an important source of RO₂ at DSL site. As for HO₂, drastic
591 decrease of ~53% was found in S1. The above-mentioned decrease in RO_x obviously could not
592 be explained solely by the remove of isoprene-related radicals. Inspection of the model results
593 shows that OVOC concentrations decreased drastically (~41%) after cutting isoprene (e.g. ~37%
594 decrease in formaldehyde, ~65% decrease in methylglyoxal, ~51% decrease in glyoxal, ~100%
595 decrease in methacrolein (MACR), and ~100% decrease in methyl vinyl ketone (MVK)). The
596 decrease in OVOC can further pull down substantial amount of primary RO₂ and HO₂ (Figure
597 6 and Figure 9). It is interesting to note that, subtracting isoprene also cause drop of NO₃
598 (~23%). This result can be contributed to the decrease of secondary production of O₃ (~35%),
599 which can further reduce the formation of NO₃, especially during nighttime.

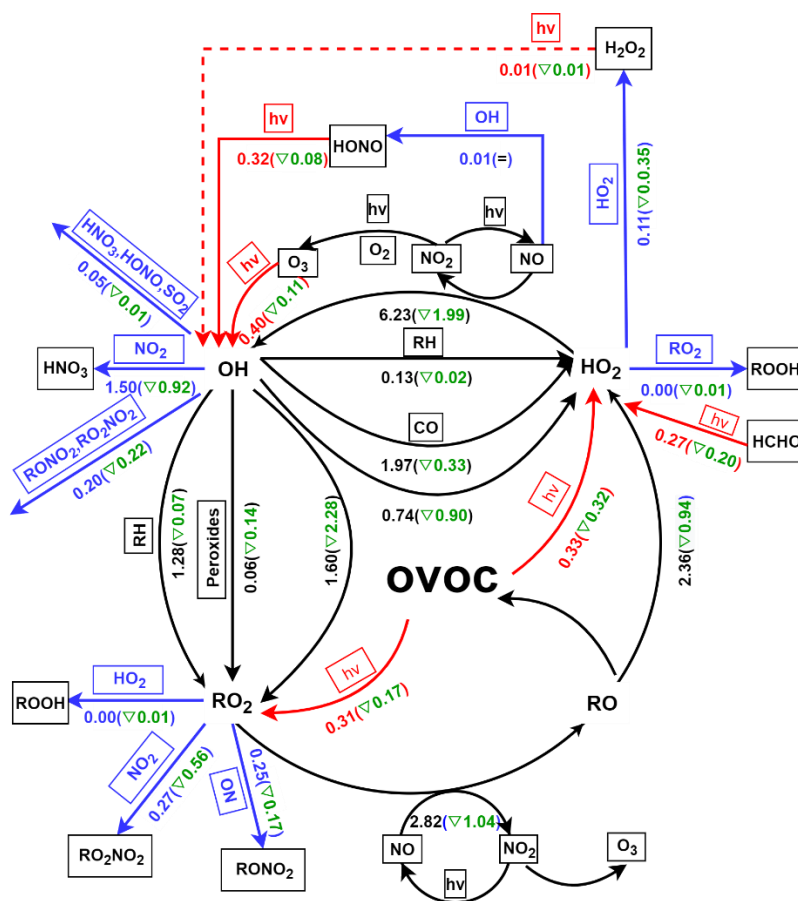


Figure 9. Summary of daytime (06:00-18:00) average budgets of RO_x radicals (in ppbv h⁻¹) in S1.

Primary RO_x sources and sinks are in red and blue, respectively, and the black lines represent the processes in RO_x and NO_x recycling. Values in the brackets represent the difference between S1 and S0.

3.6.2 Impact on O₃ formation

To investigate the detailed impact of isoprene on O₃ formation, the production and sink pathways of O₃ in S1 was also calculated (see Figure 7 (B)). In S1, the simulated maximum and daily average level of O₃ dropped to 84.95 and 41.23 ppbv, respectively, which is ~35% and ~34% lower than that in S0. Comparisons of S1 and S0 show that the absence of isoprene can reduce all the production and sink pathways of O₃. For example, the rate of the two major production pathways of O₃ (HO₂+NO and RO₂+NO) decreased by ~37% and ~45%, respectively. This can be attributed to the drop in the concentration of HO₂ and RO₂ radical in S1. As for the depletion of O₃, the absence of isoprene caused a decrease of 0.31 ppbv h⁻¹ in the reaction rate of alkene+O₃/NO₃, followed by RO₂+NO₂ (0.22 ppbv h⁻¹) and NO₂+OH

614 (0.265 ppbv h⁻¹). Apparently, the absence of isoprene will reduce the total concentrations of
615 alkenes and can further leads to the decrease of RO₂ and OH level, which ultimately slows
616 down the depletion pathways of O₃. Eventually, the absence of isoprene caused a decrease of
617 5.78 ppbv h⁻¹ in the daytime mean net production rate of O₃. Hence, isoprene chemistry plays
618 an important role in the local O₃ formation at DSL site.

619 3.6.3 Impact on HCHO formation

620 The analysis of S0 revealed the important role of isoprene, aromatics, and alkenes in the
621 production of HCHO. To investigate the chain effect of isoprene chemistry on HCHO
622 production, the major reactions that dominate the formation and depletion of HCHO in S1 were
623 also analyzed by OBM model (see Figure 8 (B)). Comparison of S0 and S1 shows that the daily
624 average HCHO decreased by 2.90 ppbv (~39%) when cutting away isoprene chemistry. It is
625 obviously that the drop in HCHO concentration cannot be solely illustrated by the absence of
626 RO (from isoprene). As aforementioned, the absence of isoprene slows down the recycling of
627 RO_x and can further lead to decrease in RO_x concentration. According to the result of OBM
628 analysis, the concentration of CH₃O, RO (from aromatics), RO (from alkanes), and RO (from
629 alkenes) decreased by 2.70×10² molecule cm⁻³, 1.59×10⁵ molecule cm⁻³, 3.35×10¹ molecule
630 cm⁻³, and 3.44 molecule cm⁻³, respectively. The drop in the HCHO precursor concentrations
631 ultimately lead to decrease in the daytime reaction rate of CH₃O + O₂, RO (from alkenes) + O₂,
632 and RO (from aromatics) + O₂ decreased by 0.66 ppbv h⁻¹ (~36%), 0.06 ppbv h⁻¹ (~16%), and
633 0.06 ppbv h⁻¹ (~40%), respectively. The total daytime formation rate of HCHO dropped to 1.71
634 ppbv h⁻¹, which was 1.66 ppbv h⁻¹ (~49%) lower than that in S0. As a result of the lower HCHO
635 and OH concentration in S1, the daily mean depletion rate of HCHO decreased by 1.25 ppbv
636 h⁻¹ (~49%). Finally, the absence of isoprene pulls down the daily average HCHO level by
637 1.61 ppbv (~36%).

638 4. Conclusions

639 Our observations at a suburban site of the YRD region from April to June in 2018 captured
640 5 typical local O₃ formation episodes. The detailed atmospheric photochemistry during these
641 episodes were analyzed. Under stagnant condition, the photolysis of OVOC served as the
642 predominant primary RO_x sources. RO_x achieves efficient recycling with the participation of
643 NO_x. Influenced by the fast RO_x recycling, local O₃ was efficiently produced and accumulated
644 under stagnant conditions. The reactions of RO radicals with O₂ dominate the photochemical
645 formation of HCHO. The higher atmospheric oxidative capacity lead to fast degradation of
646 VOCs, which can further lead to high levels of HCHO at the DSL site. Specifically, the
647 degradation of RO radicals (e.g. ISOP34O, ISOPDO, ISOPAO and ISOPBO) from isoprene
648 oxidation play an important role in the photochemical production of HCHO. To investigate the
649 role of isoprene in RO_x recycle and the formation of secondary pollutant, a sensitivity scenario
650 without isoprene (S1) input was simulated by OBM model. By comparing S1 to the standard
651 simulation (S0), we find that isoprene chemistry is important to local RO_x recycling. The
652 absence of isoprene can obviously decrease the concentrations of OVOC and the reaction rates
653 in RO_x propagations, and further reduce the concentrations of radicals (e.g. OH, HO₂, RO₂).
654 Our results indicate that the isoprene chemistry can strongly influence the formation of O₃ and
655 HCHO with the present of NO_x. Removing isoprene can slow down the reaction of HO₂+NO
656 and RO₂+NO by ~37% and ~45%, respectively, and eventually cause ~34% decrease of O₃.
657 As a result of lower O₃ concentration, average concentration of NO₃ dropped by 23% in S1.
658 The absence of isoprene can lead to decrease of RO (from isoprene) and RO_x concentration
659 and cause an obvious drop of HCHO formation (~49%). Overall, this study underlines the
660 significant role of isoprene chemistry in radical chemistry, photochemical reactions, and
661 secondary pollutant formation in the atmosphere of the YRD region and provides insights into
662 secondary pollution and its formation mechanisms.

663

664 *Data availability.* The data that support the results are available from the corresponding author
665 upon request.

666

667 *Authorship contribution.* Kun Zhang: Formal analysis, Methodology, Writing-original draft.
668 Ling Huang: Writing-review. Qing Li: Formal analysis. Juntao Huo: Formal analysis, Data
669 curation. Yusen Duan: Formal analysis, Data curation. Yuhang Wang: Writing-review.
670 Yangjun Wang: Formal analysis. Qingyan Fu: Formal analysis. Li Li: Conceptualization,
671 Methodology, Writing-review & editing.

672

673 *Competing interest.* The authors declare that they have no known competing financial interests
674 or personal relationships that could have appeared to influence the work reported in this paper.

675

676 *Acknowledgements.* This study is supported by the National Natural Science Foundation of
677 China (No.4185161), Shanghai International Science and Technology Cooperation Fund (No.
678 19230742500), and Shanghai Science and Technology Fund (No. 19DZ1205007). Y. Wang
679 was supported by the National Science Foundation. We thank Shanghai Environmental
680 Monitoring Center (SEMC) for conducting the measurement and sharing the data.

681

682

683 *Financial support.* This study was financially supported by the National Natural Science
684 Foundation of China (NO. 41875161; NO.42075144), Shanghai International Science and
685 Technology Cooperation Fund (NO. 19230742500), Shanghai Science and Technology Fund
686 (No. 19DZ1205007), Shanghai Sail Program (NO.19YF1415600), and the National Key

687 Research and Development Program of China (NO.2018YFC0213600). Y. Wang was
688 supported by the National Science Foundation.

689

690 **References**

691 Atkinson, R., and Arey, J.: Atmospheric degradation of volatile organic compounds, Chemical
692 reviews, 103, 4605-4638, 2003.

693 Atkinson, R., Baulch, D. L., Cox, R. A., Crowley, J. N., Hampson, R. F., Hynes, R. G., Jenkin,
694 M. E., Rossi, M. J., and Troe, J.: Evaluated kinetic and photochemical data for atmospheric
695 chemistry: Volume II - Gas phase reactions of organic species, Atmospheric Chemistry and
696 Physics, 6, 3625-4055, 10.5194/acp-6-3625-2006, 2006.

697 Chan, K. L., Wang, S. S., Liu, C., Zhou, B., Wenig, M. O., and Saiz-Lopez, A.: On the
698 summertime air quality and related photochemical processes in the megacity Shanghai,
699 China, Science of the Total Environment, 580, 974-983, 2017.

700 D'Ambro, E. L., Møller, K. H., Lopez-Hilfiker, F. D., Schobesberger, S., Liu, J., Shilling, J.
701 E., Lee, B. H., Kjaergaard, H. G., and Thornton, J. A.: Isomerization of second-generation
702 isoprene peroxy radicals: Epoxide formation and implications for secondary organic aerosol
703 yields, Environmental science & technology, 51, 4978-4987, 2017.

704 Gong, D., Wang, H., Zhang, S., Wang, Y., Liu, S. C., Guo, H., Shao, M., He, C., Chen, D., He,
705 L., Zhou, L., Morawska, L., Zhang, Y., and Wang, B.: Low-level summertime isoprene
706 observed at a forested mountaintop site in southern China: implications for strong regional
707 atmospheric oxidative capacity, Atmospheric Chemistry and Physics, 18, 14417-14432,
708 10.5194/acp-18-14417-2018, 2018.

709 He, Z. R., Wang, X. M., Ling, Z. H., Zhao, J., Guo, H., Shao, M., and Wang, Z.: Contributions
710 of different anthropogenic volatile organic compound sources to ozone formation at a

711 receptor site in the Pearl River Delta region and its policy implications, *Atmospheric*
712 *Chemistry and Physics*, 19, 8801-8816, 2019.

713 Jenkin, M. E., Young, J. C., and Rickard, A. R.: The MCM v3.3.1 degradation scheme for
714 isoprene, *Atmospheric Chemistry and Physics*, 15, 11433-11459, 10.5194/acp-15-11433-
715 2015, 2015.

716 Li, X., Rohrer, F., Brauers, T., Hofzumahaus, A., Lu, K., Shao, M., Zhang, Y. H., and Wahner,
717 A.: Modeling of HCHO and CHOCHO at a semi-rural site in southern China during the
718 PRIDE-PRD2006 campaign, *Atmospheric Chemistry and Physics*, 14, 12291-12305,
719 10.5194/acp-14-12291-2014, 2014.

720 Lin, H., Wang, M., Duan, Y., Fu, Q., Ji, W., Cui, H., Jin, D., Lin, Y., and Hu, K.: O₃ sensitivity
721 and contributions of different nmhc sources in O₃ formation at urban and suburban sites in
722 Shanghai, *Atmosphere*, 11, 1-18, 10.3390/atmos11030295, 2020.

723 Liu, X., Lyu, X., Wang, Y., Jiang, F., and Guo, H.: Intercomparison of O₃ formation and radical
724 chemistry in the past decade at a suburban site in Hong Kong, *Atmospheric Chemistry and*
725 *Physics*, 19, 5127-5145, 10.5194/acp-19-5127-2019, 2019.

726 Liu, Y. J., Herdlinger-Blatt, I., McKinney, K. A., and Martin, S. T.: Production of methyl vinyl
727 ketone and methacrolein via the hydroperoxyl pathway of isoprene oxidation, *Atmospheric*
728 *Chemistry and Physics*, 13, 5715-5730, 10.5194/acp-13-5715-2013, 2013.

729 Liu, Z., Wang, Y., Gu, D., Zhao, C., Huey, L. G., Stickel, R., Liao, J., Shao, M., Zhu, T., Zeng,
730 L., Amoroso, A., Costabile, F., Chang, C. C., and Liu, S. C.: Summertime photochemistry
731 during CAREBeijing-2007: RO_x budgets and O₃ formation, *Atmospheric Chemistry and*
732 *Physics*, 12, 7737-7752, 2012.

733 Riedel, T. P., Wolfe, G. M., Danas, K. T., Gilman, J. B., Kuster, W. C., Bon, D. M., Vlasenko,
734 A., Li, S.-M., Williams, E. J., Lerner, B. M., Veres, P. R., Roberts, J. M., Holloway, J. S.,
735 Lefer, B., Brown, S. S., and Thornton, J. A. (2014). An MCM modeling study of nitryl

736 chloride (ClNO₂) impacts on oxidation, ozone production and nitrogen oxide partitioning in
737 polluted continental outflow, *Atmos. Chem. Phys.*, 14, 3789–3800,
738 <https://doi.org/10.5194/acp-14-3789-2014>.

739 Tan, Z. F., Lu, K. D., Jiang, M. Q., Su, R., Wang, H. L., Lou, S. R., Fu, Q. Y., Zhai, C. Z., Tan,
740 Q. W., Yue, D. L., Chen, D. H., Wang, Z. S., Xie, S. D., Zeng, L. M., and Zhang, Y. H.:
741 Daytime atmospheric oxidation capacity in four Chinese megacities during the
742 photochemically polluted season: a case study based on box model simulation, *Atmospheric*
743 *Chemistry and Physics*, 19, 3493-3513, 2019.

744 Wennberg, P. O., Bates, K. H., Crouse, J. D., Dodson, L. G., McVay, R. C., Mertens, L. A.,
745 Nguyen, T. B., Praske, E., Schwantes, R. H., Smarte, M. D., St Clair, J. M., Teng, A. P.,
746 Zhang, X., and Seinfeld, J. H.: Gas-phase reactions of isoprene and its major oxidation
747 products, *Chemical Reviews*, 118, 3337-3390, 2018.

748 Wolfe, G. M., Kaiser, J., Hanisco, T. F., Keutsch, F. N., de Gouw, J. A., Gilman, J. B., Graus,
749 M., Hatch, C. D., Holloway, J., Horowitz, L. W., Lee, B. H., Lerner, B. M., Lopez-Hilifiker,
750 F., Mao, J., Marvin, M. R., Peischl, J., Pollack, I. B., Roberts, J. M., Ryerson, T. B.,
751 Thornton, J. A., Veres, P. R., and Warneke, C.: Formaldehyde production from isoprene
752 oxidation across NO_x regimes, *Atmospheric Chemistry and Physics*, 16, 2597-2610,
753 [10.5194/acp-16-2597-2016](https://doi.org/10.5194/acp-16-2597-2016), 2016a.

754 Wolfe, G. M., Marvin, M. R., Roberts, S. J., Travis, K. R., and Liao, J.: The Framework for 0-
755 D Atmospheric Modeling (F0AM) v3.1, *Geoscientific Model Development*, 9, 3309-3319,
756 [10.5194/gmd-9-3309-2016](https://doi.org/10.5194/gmd-9-3309-2016), 2016b.

757 Xue, L., Wang, T., Gao, J., Ding, A., Zhou, X., Blake, D. R., Fang, X., Saunders, S. M., Fan,
758 S., Zuo, H., Zhang, Q., Wang, W. Ground-level ozone in four Chinese cities: precursors,
759 regional transport and heterogeneous processes. *Atmospheric chemistry and physics*, 14(23),
760 13175-13188, 2014.

761 Xue, L., Gu, R., Wang, T., Wang, X., Saunders, S., Blake, D., Louie, P. K. K., Luk, C. W. Y.,
762 Simpson, I., Xu, Z., Wang, Z., Gao, Y., Lee, S., Mellouki, A., and Wang, W.: Oxidative
763 capacity and radical chemistry in the polluted atmosphere of Hong Kong and Pearl River
764 Delta region: Analysis of a severe photochemical smog episode, *Atmospheric Chemistry
765 and Physics*, 16, 9891-9903, 10.5194/acp-16-9891-2016, 2016.

766 Yang, X., Xue, L. K., Wang, T., Wang, X. F., Gao, J., Lee, S. C., Blake, D. R., Chai, F. H., and
767 Wang, W. X.: Observations and explicit modeling of summertime carbonyl formation in
768 Beijing: identification of key precursor species and their impact on atmospheric oxidation
769 chemistry, *Journal of Geophysic Research:Atmosphere*, 123, 1426-1440, 2018.

770 Yang, X., Zhang, G. Q., Sun, Y. M., Zhu, L., Wei, X. F., Li, Z., and Zhong, X. L.: Explicit
771 modeling of background HCHO formation in southern China, *Atmospheric Research*, 240,
772 UNSP 10494110.1016/j.atmosres.2020.104941, 2020.

773 Zeng, P., Lyu, X. P., Guo, H., Cheng, H. R., Wang, Z. W., Liu, X. F., and Zhang, W. H.: Spatial
774 variation of sources and photochemistry, of formaldehyde in Wuhan, Central China,
775 *Atmospheric Environment*, 214, 2019.

776 Zhang, K., Zhou, L., Fu, Q., Yan, L., Bian, Q., Wang, D., and Xiu, G.: Vertical distribution of
777 ozone over Shanghai during late spring: A balloon-borne observation, *Atmospheric
778 environment*, 208, 48-60, 2019.

779 Zhang, K., Li, L., Huang, L., Wang, Y., Huo, J., Duan, Y., Wang, Y., and Fu, Q.: The impact
780 of volatile organic compounds on ozone formation in the suburban area of Shanghai,
781 *Atmospheric Environment*, 232, 10.1016/j.atmosenv.2020.117511, 2020a.

782 Zhang, K., Xu, J., Huang, Q., Zhou, L., Fu, Q., Duan, Y., and Xiu, G.: Precursors and potential
783 sources of ground-level ozone in suburban Shanghai, *Frontiers of Environmental Science
784 and Engineering*, 14, 10.1007/s11783-020-1271-8, 2020b.

785 Zhu, J., Cheng, H., Peng, J., Zeng, P., Wang, Z., Lyu, X., and Guo, H.: O₃ photochemistry on
786 O₃ episode days and non-O₃ episode days in Wuhan, Central China, *Atmospheric*
787 *Environment*, 223, 10.1016/j.atmosenv.2019.117236, 2020a.

788 Zhu, J., Wang, S. S., Wang, H. L., Jing, S. G., Lou, S. R., Saiz-Lopez, A., and Zhou, B.:
789 Observationally constrained modeling of atmospheric oxidation capacity and
790 photochemical reactivity in Shanghai, China, *Atmospheric Chemistry and Physics*, 20,
791 1217-1232, 2020b.

792 Zong, R. H., Yang, X., Wen, L., Xu, C. H., Zhu, Y. H., Chen, T. S., Yao, L., Wang, L. W.,
793 Zhang, J. M., Yang, L. X., Wang, X. F., Shao, M., Zhu, T., Xue, L. K., and Wang, W. X.:
794 Strong ozone production at a rural site in the North China Plain: Mixed effects of urban
795 plumes and biogenic emissions, *Journal of Environmental Sciences*, 71, 261-270,
796 10.1016/j.jes.2018.05.003, 2018.

797

798